

Adsorption and Condensation of SO₂ in Double-Walled Carbon Nanotube Arrays Studied by Monte Carlo Simulations and Simple Analytical Models

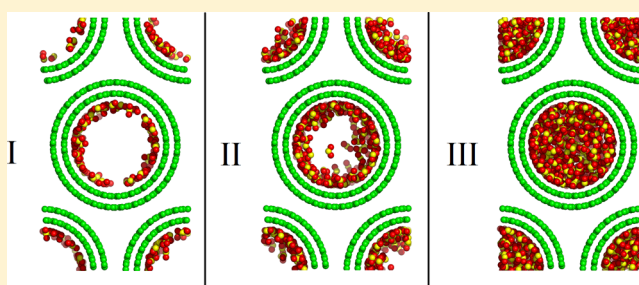
Yong-Biao Yang,^{*,†,§} Mahshid Rahimi,[†] Jayant K. Singh,^{†,‡} Michael C. Böhm,[†] and Florian Müller-Plathe[†]

[†]Eduard-Zintl-Institut für Anorganische und Physikalische Chemie, Technische Universität Darmstadt, Alarich-Weiss-Strasse 4, 64287 Darmstadt, Germany

[‡]Department of Chemical Engineering, Indian Institute of Technology Kanpur, Kanpur 208016, India

S Supporting Information

ABSTRACT: Carbon nanotubes (CNTs) have been identified as extremely promising candidates for gas capture and storage. Therefore, an understanding of the adsorption mechanisms is crucial to the improvement of CNT applications. In this work, grand-canonical Monte Carlo simulations and analytical models are used to study, at the temperature of $T = 303$ K, the adsorption and condensation of SO₂ in hexagonal arrays of double-walled CNTs of different inner nanotube radii R_{in} and intertube distances d . For both the inner and the outer adsorption, type I and type IV adsorption isotherms (IUPAC classification) are observed; they can be described adequately by analytical models. At a given pressure, the maximum adsorption among different CNT geometries depends strongly on the applied pressure. For the inner adsorption, three stages of adsorption are identified with increasing pressures. At low pressures, only one monolayer is formed, where the adsorption energy dominates the adsorption. At intermediate and high pressures, multilayers are formed until finally condensation is achieved; now it is the surface area or the available volume per CNT mass unit that dominates the adsorption. The nonlinear dependence of the outer adsorption on R_{in} and d can be explained by similar arguments as adopted for the inner adsorption. The effective number density of SO₂ molecules and isosteric heat of adsorption are also analyzed to deepen our understanding of the adsorption behavior.



1. INTRODUCTION

Since their discovery in the 1990s,^{1,2} carbon nanotubes (CNTs) have played a fundamental role in the field of nanotechnology as a result of their unique structural, mechanical, and electronic properties.^{3,4} Due to their hollow cylindrical interior, uniform structure, well-defined adsorption sites, and especially the high specific surface area of up to 1550 m² g⁻¹,^{5,6} CNTs have been identified as extremely promising candidates for gas capture and storage.^{7,8} Cinke et al. showed that purified single-walled carbon nanotubes (SWCNTs) were able to adsorb nearly twice the volume of CO₂ as activated carbon (AC).⁹ Moreover, CNTs were found to have a higher adsorption capacity, a larger adsorption energy, and a more efficient regeneration than other adsorbents.¹⁰ During the past years, numerous studies on the adsorption of different gases such as H₂, N₂, CO₂, SO₂, alkanes, and noble gases in and on closed- or open-ended SWCNTs and multiwalled nanotubes (MWCNTs) have been performed.^{7,11–35}

Due to the strong attractive van der Waals (vdW) forces between the carbon atoms of neighboring nanotubes, CNTs tend to self-assemble into stable bundles.^{14,26} Such CNT arrangements create different adsorption sites, including internal channels, grooves, and interstices between the CNTs

(see Figure 1), along with the exposed outermost surface of a bundle. The existence of distinct, easily distinguishable types of adsorption sites is a fundamental difference between CNTs and other less ordered carbon materials such as ACs. The adsorption space in CNT systems consisting of grooves and interstices, whose size depends on the nanotube radius and the intertube distance, also makes the adsorption properties tunable. An understanding of the adsorption mechanisms and the interactions between the gas molecules and the different adsorption sites is crucial to the improvement of CNT applications in gas storage and separation. Intuitively, the CNT interior is expected to have a high adsorption capacity. The attractive vdW interaction between the compounds will be maximized due to the closeness of the walls surrounding the adsorbed molecules. In contrast to this enhancement, the adsorption energy for the exterior of CNTs should be smaller than that for the interior and that for flat graphene because the outer surfaces curve away from the adsorbed molecules. This has been proven both by experiments²³ and by molecular

Received: September 13, 2015

Revised: February 20, 2016

Published: March 15, 2016

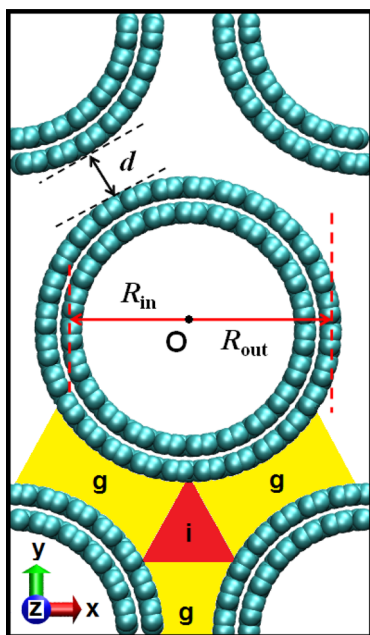


Figure 1. Schematic arrangement of a three-dimensionally aligned DWCNT array in a simulation box of volume $L_x \times L_y \times L_z \text{ nm}^3$. O labels the center of the simulation cell, R_{in} the inner nanotube radius, R_{out} the outer nanotube radius, and d the intertube distance. The length parameter d is defined as $d = d_{vdW} - \sigma_{C-C}$, where d_{vdW} measures the vdW separation between the CNT walls and σ_{C-C} the vdW diameter of carbon atoms. Interstitial and groove regions are represented by i and g, respectively. Note that there is some ambiguity on how to discriminate between i and g.

simulations²⁴ of xenon adsorption onto SWCNTs. In addition, the adsorption energy of alkanes on the groove sites of SWCNT bundles was found to lie between that for exterior and interior sites.⁷ Note that the SWCNTs used in these studies had radii less than 0.7 nm. The separation between adjacent CNTs was as small as the vdW diameter of carbon atoms.

Using density functional theory (DFT), Zhao et al.²⁶ studied the adsorption of various gases on SWCNTs and bundles of them. They observed a better adsorption on interstitial and groove sites of the bundles than on individual CNTs. Wongkoblak et al.²⁸ investigated the adsorption of argon and nitrogen in a bundle of SWCNTs by grand-canonical Monte Carlo (GCMC) simulations. Adsorption sites including the interior, cusp interstices inside the bundles, and square interstices outside the bundles were considered. Their results showed that for the CNTs with nanotube radii less than 0.54 nm, adsorption of argon and nitrogen occurred mainly in the CNT interior. In CNTs with nanotube radii between 0.54 and 0.82 nm, adsorption occurred first in the small cusp interstices and then—when the pressure is increased—in the square interstices.

Bienfait et al.²⁷ used adsorption isotherms, the isosteric heat of adsorption, and neutron diffraction measurements of different gases to study the adsorption on SWCNT bundles. They showed that grooves were the most preferable sites for adsorption. This result was confirmed by molecular dynamics (MD) studies³¹ and GCMC simulations.^{17,18} By investigating the adsorption of propane and propylene on homogeneous SWCNT bundles, Cruz et al.³¹ found that for nanotube radii larger than 0.74 nm, the low-pressure adsorption started in the grooves. Only after completely filling the grooves, the

adsorption proceeded in other regions of the outer surface of CNTs. Kowalczyk et al.¹⁷ showed that the nanotube radius for the maximum adsorption of CO_2 in CNT bundles depends on the applied pressure and that the selectivity of CO_2 adsorption varies with the intertube distance. Rahimi et al.^{18,32} studied CO_2 adsorption in double-walled carbon nanotube (DWCNT) arrays of nanotube radius 2.5 nm with different intertube distances d . They found that both the preferential adsorption sequence at different adsorption sites and the maximum adsorption at a given pressure p depend on the intertube distance and the applied pressure. A similar dependence on d and p was also found in recent GCMC simulations of Rahimi et al.,³² where the adsorption of SO_2 in DWCNT arrays was studied under pressures from 0.01 to 2.5 bar.

In addition to experiments and simulations, analytical theory has also contributed to a better description of adsorption isotherms. Classical models have been developed by Langmuir,³⁶ Freundlich,³⁷ Brunauer, Emmett, and Teller (BET),³⁸ and others (for a detailed review, see ref 39). Specifically, for gas adsorption in CNTs, new models have been proposed.^{15,16,22,40} Arora et al. suggested a double Langmuir model leading to an accurate description of the inner N_2 adsorption on SWCNTs.⁴⁰ Taking into account the curvature effect of CNT walls⁴¹ and postulating a layer-by-layer mechanism in the BET theory,³⁸ Furmaniak et al. proposed several simple analytical models for describing the inner and outer adsorption in SWCNTs or MWCNTs.^{15,16} They found that the adsorbate–adsorbate interactions cannot be neglected in the description of adsorption. In order to avoid time-consuming iterative procedures in the fitting calculations, another much simpler analytical model was also developed, which combines the layer-by-layer mechanism and an empirical formula.²² The models proposed by Furmaniak et al. provided an accurate description of the N_2 ^{15,16} and CCl_4 ²² adsorption isotherms.

On the basis of the available literature, the state of art in this field can be summarized as follows: (1) Due to the uncontrollable release of flue gas accompanied by the rapid development of global industry during the last decades, the use of CNTs to adsorb pollutants has become important in both fundamental and practical research. Hitherto, most studies have been carried out for CO_2 capture and separation because it is the major component of flue gas and causes the greenhouse effect. In contrast, only limited studies exist for SO_2 , although it is also contained in flue gas and contributes to acid rain. (2) In most studies, SWCNTs were used instead of MWCNTs. A possible reason might be that their adsorption capacity is higher than that of MWCNTs.¹² However, SWCNTs are still expensive and difficult to synthesize. In fact, DWCNTs have become an attractive alternative since their properties are similar to those of SWCNTs.^{29,42} (3) Only adsorption processes at pressures much lower than the saturation vapor pressure (p_s) were studied in the majority of publications.³² At high pressures, gas adsorption within CNT bundles may lead to condensation, a phenomenon with potential additional applications in sensor technology.⁴³

In the present contribution, we perform GCMC simulations to study SO_2 adsorption in three-dimensional (3D) highly aligned arrays of DWCNTs at pressures reaching 98% of p_s . To investigate the role of the geometry of CNT arrays, several different nanotube radii and intertube distances are considered. For both inner and outer adsorption, the adsorption isotherms are determined by simulations as well as by analytical models.

The gravimetric adsorption capacity is analyzed as a function of the nanotube radius and intertube distance. The adsorption sequence is explained according to the different stages of adsorption processes. Furthermore, to obtain an understanding of the combined effect of CNT curvature and the volume of the adsorption space, the capacities of the accessible adsorption sites in CNT arrays are also discussed comparatively with the help of the effective number density of SO₂ and the isosteric heat of adsorption.

2. MODEL AND METHOD

Dense arrays of highly aligned DWCNTs²⁹ are modeled and arranged in a hexagonal lattice. They are described by a periodic simulation box of size $L_x \times L_y \times L_z$ nm³, as shown in Figure 1. Armchair CNTs of inner nanotube radii from 1 to 4 nm, lengths fixed to $L_z = 4.919$ or 3.443 nm, and intertube surface-to-surface distances between $d = 0$ and 2 nm are investigated at 303 K. More structural details are given in Supplementary Table S1. The rigid CNTs are described by a Lennard–Jones potential as defined in the AMBER 96 force field ($\epsilon_{C-C} = 0.36$ kJ/mol, $\sigma_{C-C} = 0.34$ nm),⁴⁴ which has been used also in similar studies.^{18,32,45}

The SO₂ molecules are modeled by the parameters developed by Ketko et al., which are tuned to reproduce the vapor–liquid equilibria, critical properties, the vapor pressure, and heats of vaporization with high accuracy.⁴⁶ In the adopted force field, SO₂ is described as a 3-site rigid molecule with Lennard–Jones interactions and partial charges ($\sigma_{S-S} = 0.339$ nm, $\epsilon_{S-S} = 0.61361$ kJ/mol, $\sigma_{O-O} = 0.305$ nm, $\epsilon_{O-O} = 0.65684$ kJ/mol, $q_S = +0.590$ e, $q_O = -0.295$ e). The O and S atoms are connected by rigid bonds with a length 0.1432 nm. The O–S–O bond angle is fixed at 119.3°. The Lorentz–Berthelot mixing rules $\epsilon_{ij} = (\epsilon_i \epsilon_j)^{1/2}$ and $\sigma_{ij} = (\sigma_i + \sigma_j)/2$ are used to calculate the dissimilar nonbonded interactions.⁴⁷ The smooth particle-mesh Ewald method is used for the electrostatic interactions.⁴⁸

The GCMC method has been applied to derive the adsorption isotherms at constant temperature T , chemical potential μ , and volume V . The pressures studied in this work come close to the saturation vapor pressure of SO₂ at 303 K, $p_s = 4.6$ bar.^{49,50} To take into account the nonideal behavior of the SO₂ gas, the chemical potential μ is derived from fugacity data and calculated by the Peng–Robinson equation of state⁵¹ with a critical temperature $T_c = 431.6$ K and a critical pressure $p_c = 79.2$ bar.⁴⁶

For all simulation runs, 5×10^7 Monte Carlo steps are used for both equilibration and production periods. Three types of Monte Carlo moves are employed: displacement, rotation, and insertion/removal, with relative trial probabilities of 0.2, 0.1 and 0.7, respectively. During the equilibration, the maximum allowed displacement and rotation of the molecules is adjusted so that one-half of the trial moves are accepted.

The GCMC simulation output provides the total number of SO₂ molecules in the simulation box, which is denoted as absolute adsorption N_{ad} . For a convenient comparison with experimental results, we converted N_{ad} into the gravimetric adsorption n_{ad} with a frequently used unit, mmol/g, i.e., millimole of SO₂ per gram of CNT. In this contribution the adsorption amount is always defined as gravimetric adsorption.²⁰ To investigate the volumetric adsorption, the effective number density of SO₂, ρ^{eff} , is used and evaluated as

$$\rho^{eff} = N_{ad}/V^{free} \quad (1)$$

where V^{free} is the free volume in a given CNT array, i.e., the volume not occupied by CNTs (see Appendix A). The derivative of the adsorption energy with respect to the absolute adsorption, which is called the isosteric heat of adsorption, q_{st} , reflects the strength of the adsorbent–adsorbate interaction. Approximately, it can be calculated as

$$q_{st} \approx RT - \left(\frac{\partial U_{ad}}{\partial N_{ad}} \right)_{T,V} \quad (2)$$

where R is the gas constant and U_{ad} the intermolecular energy of the system.⁵² With this sign convention, a higher value of q_{st} signifies stronger adsorption. Using fluctuation theory, eq 2 can be brought into the form used here

$$q_{st} \approx RT - \frac{\langle U_{ad} N_{ad} \rangle - \langle U_{ad} \rangle \langle N_{ad} \rangle}{\langle N_{ad}^2 \rangle - \langle N_{ad} \rangle^2} \quad (3)$$

where the notation $\langle \dots \rangle$ represents ensemble averaging.

3. MODEL FORMULATION

In this work, simple analytical models are used to fit the obtained adsorption isotherms. Since the details of these models can be found elsewhere,^{15,16,22} we discuss them here only briefly. The nanotube (NT) version of the polymolecular Fowler–Guggenheim (NT-PFG) model assumes a layer-by-layer adsorption mechanism as in the BET theory.^{15,16} Due to the strong adsorbate–adsorbent interactions, it is assumed that the creation of the first layer can be treated independently from the formation of the additional layers. Since a proper description of the monolayer state is only possible if the lateral adsorbate–adsorbate interactions are taken into account,^{15,16} one derives for the relative pressure

$$\frac{p}{p_s} = \frac{\Theta_i}{K_i^{FG}(1 - \Theta_i)} \exp(-A\Theta_i) \quad (4)$$

where A is related to the interaction between molecules adsorbed on adjacent sites and i is the number of layers. Θ_i and K_i^{FG} symbolize the coverage of the i th layer and the Fowler–Guggenheim constant, respectively. As the interactions between adsorbed molecules in the second and the first layers are of the same kind as those between the $(i + 1)$ th and the i th layers ($i > 1$) (i.e., the adsorbate–adsorbate interaction), the corresponding Fowler–Guggenheim constants are assumed to be identical. As a result, for $i = 1$ we have $\Theta_i = a_1/a_m$, $K_i^{FG} = K_1^{FG}$, while for $i > 1$ those definitions read $\Theta_i = a_i/(\alpha_{i-1}a_{i-1})$ and $K_i^{FG} = K_p^{FG}$. Here, a_m is the maximum monolayer capacity in the first layer, and a_i is the adsorption amount actually achieved in the i th layer. K_1^{FG} and K_p^{FG} are two parameters with fixed values. An additional parameter α_i characterizes the geometry of the adsorption space. For the inner adsorption in CNTs, an adsorption space with cylindrical geometry is assumed. The first layer is adsorbed directly on the CNT wall, while the $(i + 1)$ th layer is adsorbed on the i th layer. In other words, the bottom surface of the i th layer is the interface between the i th and the $(i - 1)$ th layers and the upper surface of the i th layer is the interface between the i th and the $(i + 1)$ th layers. As a result, the area of the upper surface of the i th layer should be smaller than its bottom surface by a factor

$$\alpha_i = \frac{R_{in}^{eff} - i \cdot \lambda}{R_{in}^{eff} - (i - 1) \cdot \lambda} = \frac{1 - i \cdot \lambda/R_{in}^{eff}}{1 - (i - 1) \cdot \lambda/R_{in}^{eff}} \quad (5)$$

where R_{in}^{eff} is the effective inner radius of the CNT (see Appendix A) and λ is the layer thickness. Thus, we have the maximum number of layers, $N_{layer} \leq R_{in}^{eff}/\lambda$, which in this definition is an integer. Similarly, for the outer adsorption, which employs the effective outer radius of the CNT, R_{out}^{eff} (see Appendix A), eq 5 is modified to

$$\alpha_i = \frac{R_{out}^{eff} + i \cdot \lambda}{R_{out}^{eff} + (i - 1) \cdot \lambda} = \frac{1 + i \cdot \lambda / R_{out}^{eff}}{1 + (i - 1) \cdot \lambda / R_{out}^{eff}} \quad (6)$$

However, in the work of Furmaniak et al.,²² only isolated CNTs were treated and N_{layer} is an optimized integer number to allow best fitting. This means that all adsorption layers are regarded as completely filled and no adsorption in the interstitial regions is considered. In our model systems, the geometry of the adsorption space is well defined and the adsorption layers in the interstitial regions are included (see Figure A1). The adsorption in the interstitial regions is evaluated by introducing another multiplier, c_w , into eq 6 (see Appendix B). Thus, the suggested modified NT-PFG model for the outer adsorption allows for adsorption on all possible sites.

In an alternative way, using eq 4 for the first layer and assuming that the formation of higher layers is mainly driven by the adsorbate–adsorbate interactions, Furmaniak et al. proposed a nanotube version of the generalized D’Arcy and Watt (NT-GDW) model.²² In this description all adsorptions except those in the first layer are evaluated by using an empirical formula (of course, many options are available^{53,54})

$$a_{multilayer} = \frac{c \cdot w \cdot a_1 \cdot p/p_s}{1 - c \cdot p/p_s} \quad (7)$$

where w is a parameter determining which fraction of the molecules in the i th layer migrates into the $(i + 1)$ th layer. Quantity c is a parameter to describe adsorption in the subsequent layers. Therefore, the total adsorption amount, a , is a sum of mono- and multilayer contributions

$$a = a_1 + a_{multilayer} \quad (8)$$

Furthermore, the heterogeneity of CNT walls is also taken into account. It originates from the patches of different adsorption capacities on CNT walls. The patches are distinguished and characterized by different adsorbate–adsorbent interaction energies. Thus, a patchwise NT-GDW model was developed by using eqs 4, 7, and 8 along with

$$a_1 = \sum_j a_{1,j} \quad (9)$$

where $a_{1,j}$ is the first-layer adsorption on patch j .²² The advantage of the NT-GDW model is its conceptual simplicity. Although its application is computationally less time consuming than that of the NT-PFG model, it is expectedly less successful to provide an unambiguous picture as the NT-PFG model based on a layer-by-layer adsorption mechanism. When mentioning the NT-GDW model in the next section, we always use the patchwise approach taking into account two patches (i.e., $a_1 = a_{1,1} + a_{1,2}$).

4. RESULTS AND DISCUSSION

In the present work, two limiting cases of SO_2 adsorption have been the focus of our research: inner adsorption where only the CNT interior is accessible and outer adsorption in completely closed CNTs where adsorption can only take place in the space

between the CNTs such as interstitial and groove regions. The unrestricted adsorption in all regions mentioned above can be described as a simple sum of inner and outer adsorption processes (see Supplementary Figure S1(a)), as also observed by Rahimi et al. for CO_2 adsorption in DWCNT arrays at pressures less than 40 bar.¹⁸ These findings are of practical significance, as they offer convenient access to the unrestricted adsorption by simply summing the data for inner and outer adsorptions. Moreover, as the inner and outer processes do not influence each other significantly, it is more convenient to understand the corresponding adsorption mechanisms separately.

Furthermore, we found that the inner adsorption does not depend on the intertube distance d (see Figure S1(b)). Therefore, we restricted the discussion of the inner adsorption to $d = 0.3$ nm. In order to save computational time, a nanotube length, $L_z = 3.443$ nm, is used in connection with $R_{in} = 4.001$ nm. The adsorption isotherms are insensitive to further increase in the CNT length (see Figure S1(c)).

4.1. Inner SO_2 Adsorption in DWCNT Arrays. Figure 2 presents the isotherms of inner adsorption for different

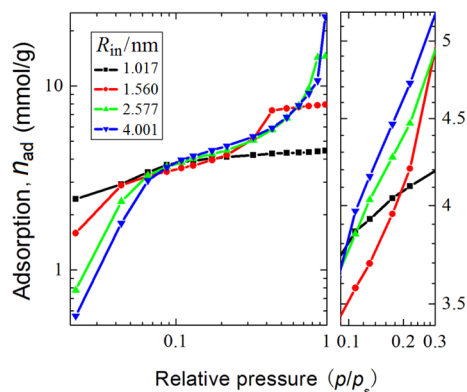


Figure 2. Inner adsorption isotherms of SO_2 in DWCNT arrays with different inner nanotube radii R_{in} . The adsorption in an intermediate pressure region is shown on the right in an enlarged scale. All solid lines are given as a guide for the eye.

nanotube radii. It can be seen that for relative pressures of $p/p_s < 0.05$, the gravimetric adsorption n_{ad} decreases with increasing R_{in} . While for intermediate pressures ($0.1 < p/p_s < 0.3$, see the right enlarged diagram of Figure 2), the gravimetric adsorption n_{ad} increases with increasing R_{in} (here the sample with $R_{in} = 1.017$ nm is an exception, which will be discussed below). When the relative pressure is larger than 0.3, the largest adsorption is achieved first at $R_{in} = 1.560$ nm, then at $R_{in} = 2.577$ nm, and finally at $R_{in} = 4.001$ nm, i.e., R_{in} for the maximum adsorption at a given pressure gradually increases with the applied pressure. Thus, the nanotube radius is an important parameter to tailor the adsorption capacity of CNTs. Some authors claimed that an increasing nanotube radius implies an increase in pure gas adsorption,⁵⁵ while others argued that the optimal nanotube radius for maximum adsorption depends on the applied pressure.^{18,32,56} This uncertainty might originate from the fact that in some works only a limited number of nanotube radii or pressure values were considered. Our results confirm that the nanotube radius for maximum adsorption depends on the applied pressure.

The result shown in Figure 2 can be well understood by measuring the effective number density of SO_2 as a function of

the applied pressure (Figure 3) and the density profile of sulfur atoms as a function of the distance from the nanotube wall

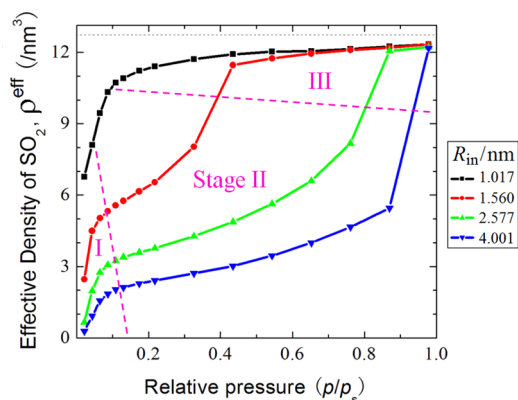


Figure 3. Effective SO_2 density for the inner adsorption in DWCNT arrays of different nanotube radii R_{in} as a function of pressure. The upper black dashed line represents the SO_2 bulk density at the saturation pressure (4.6 bar). The curves are divided into three pressure-controlled stages. The vertical dashed line separates stages I and II, while the horizontal one separates stages II and III. Solid lines are given as a guide for the eye. Note that although stage II seems to be absent in the black curve with $R_{\text{in}} = 1.017$ nm, it exists. This can be verified by the isosteric heat of adsorption given in Figure 6.

(Figure 4). In Figure 3 we show that each adsorption isotherm can be divided into three stages. In stage I the effective number density ρ^{eff} increases quickly with the pressure; then in stage II ρ^{eff} increases not as fast as in stage I (the sample with $R_{\text{in}} = 1.017$ nm is an exception, as discussed below). After a sharp increase of ρ^{eff} , it enters stage III where ρ^{eff} increases very slowly and gradually approaches an asymptotic value, i.e., the SO_2 bulk density at the saturation pressure.

In stage I, which occurs at low pressures, only one incompletely filled adsorption layer is formed, as can be seen from Figure 4 with $p/p_s = 0.022$. The gas molecules are directly adsorbed to the inner wall of the CNTs. Here the adsorbate–adsorbent interaction dominates the adsorption, and the CNT curvature plays a dominant role: the smaller the nanotube radius is, the larger is the adsorption energy.²⁴ As a result of this effect, the adsorbate density in the monolayer decreases strongly with increasing nanotube radius. Thus, the gravimetric adsorption n_{ad} also decreases monotonically with increasing nanotube radius, especially at very low pressures. This trend is roughly conserved until the first layer is almost formed. When measured in the form of the effective density ρ^{eff} , see Figure 3 within the range of stage I, the monotonic decrease of ρ^{eff} with increasing R_{in} is even more remarkable. For example, at $p/p_s = 0.022$, the values of n_{ad} for $R_{\text{in}}/\text{nm} = 1.017$ and 4.001 shown in Figure 2 is 2.435 and 0.562 mmol/g (the ratio is 1:0.231), respectively. On the other hand, ρ^{eff} for $R_{\text{in}}/\text{nm} = 1.017$ and 4.001 (see Figure 3) amounts to 6.764 and 0.287/nm³ (the ratio is 1:0.042), respectively. The sharp decrease in ρ^{eff} at higher R_{in} can be explained by the larger empty space with increasing R_{in} when only a monolayer is formed in stage I.

For a further verification of the CNT curvature effect, consider the $p/p_s = 0.022$ curve (i.e., the bottom curve) in Figure 4 as an example. For $R_{\text{in}} = 1.017$ nm (see Figure 4a), the peak in the number density of the first layer (denoted as ρ_{bot}) is already more than 70% of that at $p/p_s = 0.978$ (i.e., the top curve, and this peak maximum is denoted as ρ_{top}) and about

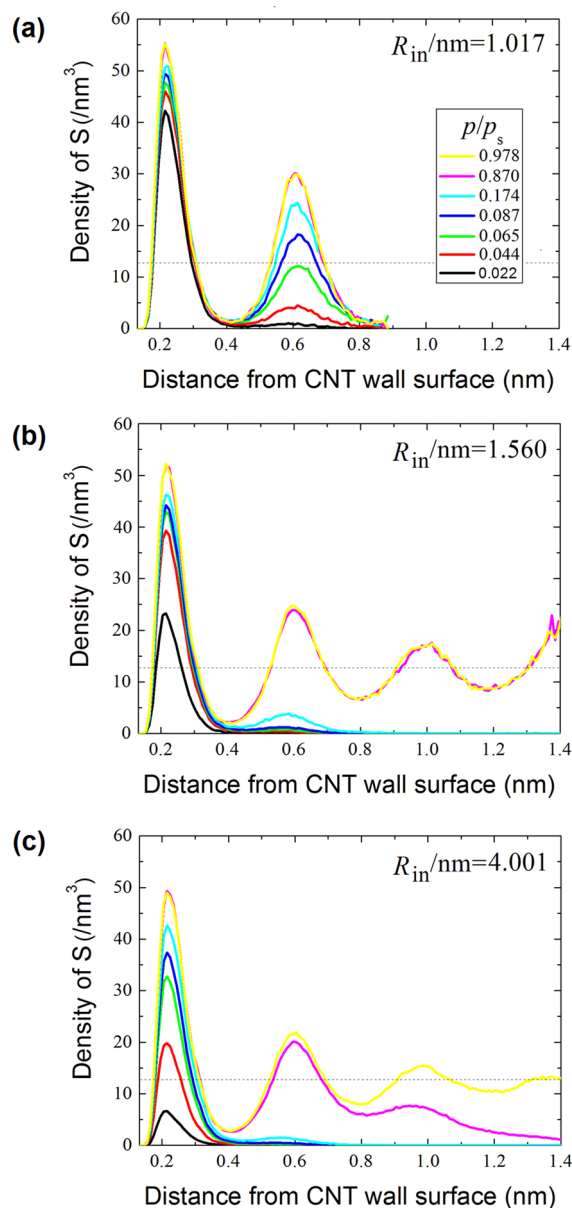


Figure 4. Density profiles of the S atoms for the inner adsorption in DWCNT arrays with different nanotube radii R_{in} . The normalized pressure p/p_s increases from the lowest to the highest curve. Dashed line represents the SO_2 bulk density at the saturation pressure, 4.6 bar.

three times as large as at the saturation density under bulk conditions (denoted as ρ_s). For $R_{\text{in}} = 1.560$ nm (see Figure 4b), ρ_{bot} is only slightly smaller than 50% of ρ_{top} and about two times as large as ρ_s . The curvature effect implies that for $R_{\text{in}} = 4.001$ nm (see Figure 4c) the value of ρ_{bot} is even smaller than those encountered at smaller R_{in} .

In stage II, which takes place at intermediate pressures, the first layer has been almost completely formed and multiple higher layers are being formed, as can be seen from Figure 4 with $p/p_s = 0.174$ for $R_{\text{in}} = 1.560$ and 4.001 nm. Since the first layer has been almost completely formed (note that for different R_{in} the densities of adsorbate molecules in an almost completely formed first layer are very close to each other. See the maximum values of those first peaks in Figure 4 with $p/p_s = 0.174$), the adsorption of gas molecules is now mainly determined by the adsorbate–adsorbate interaction. However,

with an increasing number of layers, the influence of the curvature of the CNT walls becomes continuously weaker. As a result, the density of adsorbate molecules in the i th ($i > 1$) layer is almost independent of the nanotube radius. Thus, now it is the surface area per CNT mass unit that dominates the adsorption. The maximum amount of adsorption is achieved for the largest R_{in} value, i.e., for the smallest curvature. That is the reason why in Figure 2, for intermediate pressures, n_{ad} increases with increasing R_{in} when $R_{in} > 1.017$ nm. However, ρ^{eff} still decreases with increasing R_{in} for intermediate pressures (see Figure 3). This is attributed to the increasing amount of empty space with increasing R_{in} , reducing ρ^{eff} significantly.

In stage III, which requires higher pressures, the whole space in the CNT interior gets almost saturated after the condensation transition. Increasing pressure can only lead to an insertion of additional gas molecules into the filled layers. Now the adsorption amount gradually approaches an asymptotic value. Thus, the adsorbate density in the CNT interior for all R_{in} is very close to the bulk density at the saturation pressure, as can be seen in Figure 3. In this situation a similar argument as formulated for stage II can be applied also for stage III, i.e., the gravimetric adsorption increases monotonically with the volume of the adsorption space confined to a CNT mass unit. Hence, at a given pressure within stage III the maximum gravimetric adsorption n_{ad} is achieved with the largest nanotube radius.

It is also evident from Figure 3 that the systems with larger R_{in} undergo capillary condensation at higher pressures. A further verification is possible with the help of the boundary between stages II and III, which can be represented by an almost “horizontal” separator, while the other boundary, i.e., the one between stages I and II, appears as a “vertical” separator. Thus, the optimal nanotube radius R_{in} for the maximum adsorption is the largest R_{in} for the already saturated systems at given pressures, as shown in Figure 2 for high pressures of $p/p_s > 0.3$. To give an example, when the system of $R_{in} = 1.560$ nm is already saturated while the systems of $R_{in} > 1.560$ nm is not, $R_{in} = 1.560$ nm is the optimal nanotube radius for the maximum adsorption. This is also true with $R_{in} = 2.577$ nm. Again, we show that the relation between the adsorption sequence and the nanotube radius depends on the applied pressure.^{18,32,56}

We mentioned above that the sample of $R_{in} = 1.017$ nm is an exception as discussed for Figure 2. Nevertheless, the adsorption isotherm for $R_{in} = 1.017$ nm can also be divided into three stages, as shown in Figure 3, although it seems only two stages exist. This can be explained as follows. The inner adsorption space of a CNT with $R_{in} = 1.017$ nm can accommodate at most 2 layers of SO_2 , as can be extracted from Figure 4a and more intuitively from Figure 5. Due to the high adsorption energy caused by the large curvature of the CNT wall and the limited adsorption space, the monolayer is already almost complete at extremely low pressures. Then we see a quick saturation at a very low pressure. In other words, for $R_{in} = 1.017$ nm, both stages I and II cover a very small pressure range, over which most of the adsorption process occurs. Under the same applied pressures, $0.1 < p/p_s < 0.3$, systems with $R_{in} > 1.017$ are mostly in stage II of the adsorption process (see Figures 3 and 5), while the system with $R_{in} = 1.017$ nm has already entered stage III, i.e., the condensed state with a very high density. As a result, the gravimetric adsorption n_{ad} for $R_{in} = 1.017$ nm is not the lowest as shown in the right enlarged diagram of Figure 2. This also explains that for $R_{in} = 1.017$ nm

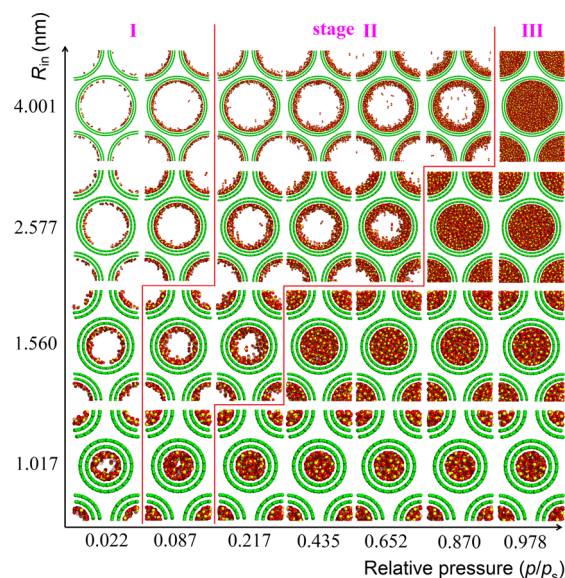


Figure 5. Snapshots for the inner adsorption of SO_2 molecules in DWCNT arrays of different nanotube radii R_{in} as a function of the pressure. The snapshots are divided into three groups according to the three adsorption stages.

we see a type I isotherm, while for $R_{in} > 1.017$ nm adsorption isotherms of type IV are obtained.⁵⁷

To summarize, the pressure dependence of an adsorption process can be divided into three stages: (I) a monolayer being formed, (II) the increase in the number of adsorption layers, and (III) the insertion of SO_2 into an already filled adsorption space after the condensation transition. Note that under a given applied pressure, the stage of an adsorption isotherm may be different for different R_{in} values. For these stages, the CNT curvature (or the adsorption energy), the surface area, or the available volume per CNT mass unit dominate the adsorption, respectively. This agrees very well with the conclusion from the GCMC simulations of hydrogen uptake in metal–organic frameworks, although different adsorbate and adsorbent were used.⁵⁸

The three stages are also visible in the isosteric heat of adsorption, q_{st} as shown in Figure 6. According to eqs 2 and 3, q_{st} is related to the derivative of the adsorption energy with

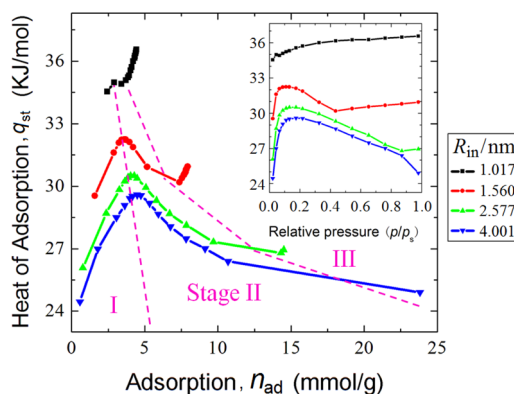


Figure 6. Isosteric heat of adsorption for the inner SO_2 adsorption in DWCNT arrays with different nanotube radii R_{in} as a function of gravimetric adsorption (in the inset the pressure dependence of the gravimetric adsorption is presented). Solid lines are given as a guide for the eye.

respect to the adsorption amount. Thus, q_{st} reacts sensitively on changes of the adsorption energy. Figure 6 emphasizes again that for $R_{in} = 1.017$ nm stages I and II are limited to a small window of the gravimetric adsorption. The occurrence of stage III cannot be identified unambiguously for $R_{in} = 4.001$ nm, although we believe that it will occur in simulations with more data points. To shorten the discussion, here we take the $R_{in} = 1.560$ nm system as an example. At lower pressures (hence, lower adsorption), i.e., under stage I conditions, q_{st} increases as a function of pressure (adsorption amount). During the formation of the monolayer and if only adsorbate–adsorbent interactions contribute to the adsorption energy, q_{st} would be approximately constant. In contrast to this simplifying assumption, adsorbate–adsorbate interactions also contribute to the adsorption energy. They become stronger with increasing adsorbate density in the first adsorption layer and thus with the decrease of the adsorbate–adsorbate distance. As a net effect in stage I, the participation of both kinds of interactions causes an increase of q_{st} with increasing pressure. In stage II, multiple layers gradually form. The SO_2 molecules adsorbed in the i th layer ($i > 1$) are not in direct contact with the CNT walls. Even under the assumption that the contribution of the adsorbate–adsorbate interaction is identical to the one in the first layer, now the increase of the total adsorption energy with the adsorption amount is smaller than the linear enhancement observed in stage I. This leads to the situation that q_{st} is reduced with an increasing number of layers. After having filled the whole adsorption space and the subsequent condensation, increasing pressure only allows the insertion of additional SO_2 molecules, with a slight increase in the adsorption amount. Now q_{st} starts to increase again, which implies that the adsorbate–adsorbent interactions or the adsorbate–adsorbate interactions are enhanced. The same argument can be also applied to other samples despite the fact that some stages are not significant.

4.2. Outer SO_2 Adsorption in DWCNT Arrays. As a result of stronger spatial variations in the adsorption space, depending on both nanotube radius and intertube distance, the outer adsorption is more complex than the inner. Although the adsorption capacity of CNTs depends on both R_{out} and d , the latter quantity has been identified as the more important influencing parameter because it can be tuned more easily. Since R_{out} is always 0.339 nm larger than R_{in} (see Table S1) and in order to keep systems identifiable, we confine to classify them by their R_{in} . Figure 7 presents the outer adsorption isotherms of SO_2 for different nanotube radii and intertube distances. The maximum adsorption for a given CNT radius is seen for the largest value of d considered in this work, at a pressure close to p_g . This trend is essentially the same as that in the case of the inner adsorption at high pressures, where, after the condensation transition, the available volume dominates the adsorption amount.

At smaller intertube distances, $d = 0.0$ and 0.2 nm, the limited space in the interstitial region and the grooves hinders the outer adsorption in the samples. For these intertube distances, the adsorption space is formed by extremely narrow pores. On the basis of the distance between two density peaks in Figure 4, the layer thickness for SO_2 adsorption is estimated to be $\lambda \approx 0.3$ nm. Hence, SO_2 molecules are adsorbed simultaneously on two or three CNT walls (see Figure 8 for an example), which leads to large adsorption energies. However, the small adsorption volume is filled already at extremely low pressures. As expected, the samples with small CNT

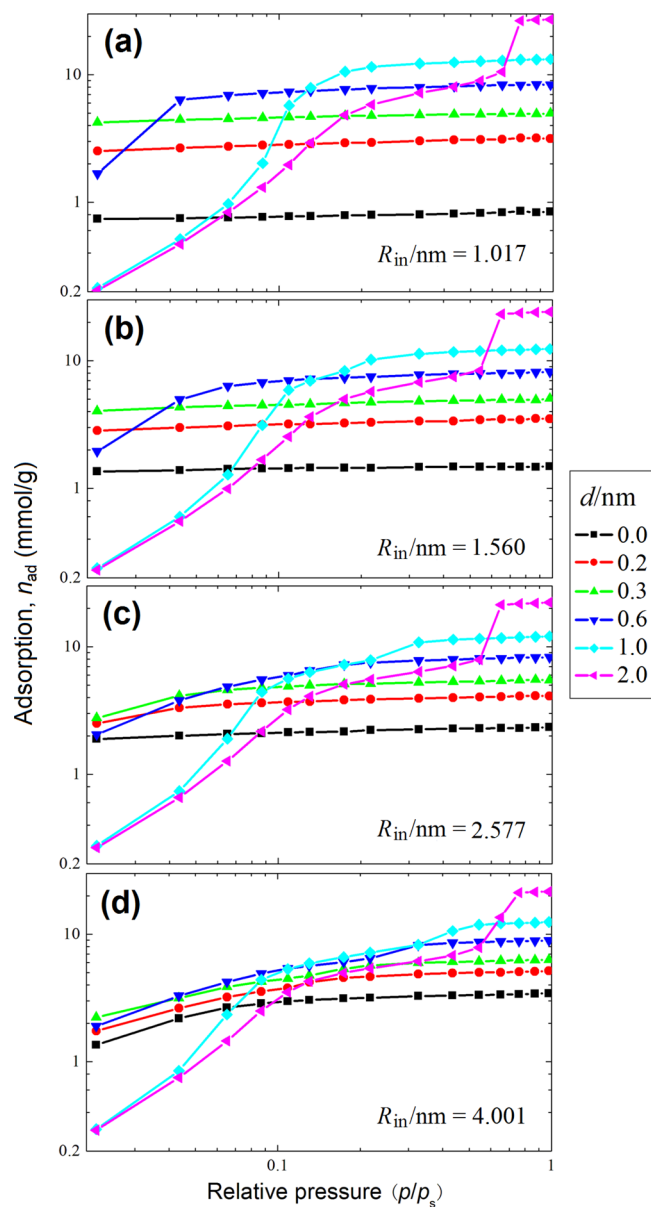


Figure 7. Outer adsorption isotherms of SO_2 in DWCNT arrays with different nanotube radii R_{in} and intertube distances d . Solid lines are used as a guide for the eye.

separations are characterized by a combination of limited adsorption space and large adsorption energy. Therefore, even at very low pressures, the maximum adsorption is achieved for $d = 0.3$ nm, as shown in Figure 7a–d. Here the intertube distance $d = 0.3$ nm leads to a similar adsorption energy as encountered for $d = 0.0$ and 0.2 nm. However, the adsorption space of the former case is larger. This has been also observed by Rahimi et al. under low pressures.³²

It can be concluded that the outer adsorption is influenced by the combined effect of nanotube radius and intertube distance. From Figure 9 we recognize that the adsorption amount is not always changing monotonically as a function of R_{in} or d . Let us consider first the behavior under low-pressure conditions (Figure 9a). Only for $d = 0.3$ nm and $d \geq 1.0$ nm the adsorption amount is a monotonic function of R_{in} . In the former case it decreases as a function of R_{in} , while in the latter case it increases. For all nanotube radii, the maximum

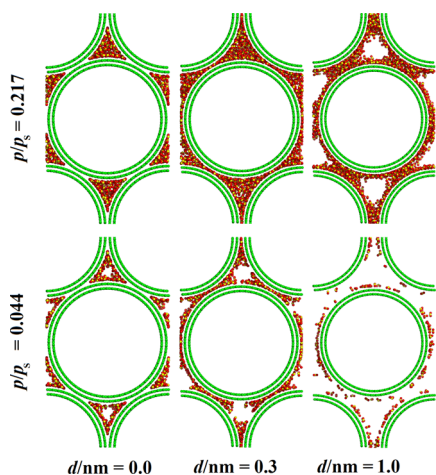


Figure 8. Snapshots of the outer adsorption of SO_2 molecules in DWCNT arrays with an inner nanotube radius $R_{\text{in}} = 4.001$ nm for different relative pressures and intertube distances.

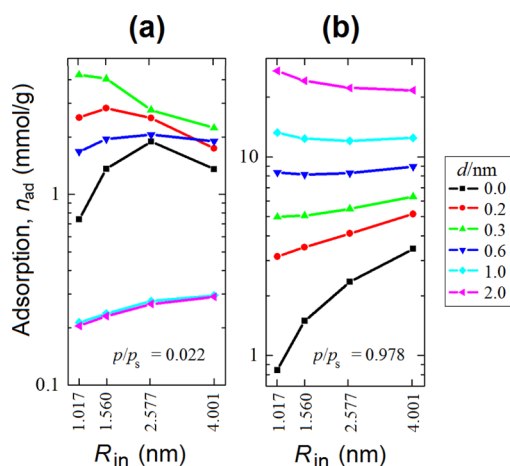


Figure 9. Outer adsorption of SO_2 in DWCNT arrays as a function of the nanotube radius R_{in} for different intertube distances d . Two different normalized pressure ratios have been considered: (a) $p/p_s = 0.022$ and (b) $p/p_s = 0.978$. Solid lines are used as a guide for the eye.

adsorption is always found at an intertube distance of $d = 0.3$ nm. This can be traced to the monolayer formation in the grooves (see Figure 8). In this region, the adsorption energy is maximized due to the high density of CNT carbon atoms.²⁷ At high pressures, however, when the gas has condensed, the available volume determines the adsorption capacity. It is found from Figure 9b that for any chosen R_{in} the gravimetric adsorption increases with d , but for a given d it does not always increase with R_{in} . If d is small (i.e., $d \leq 0.3$ nm) the maximum adsorption occurs for the largest R_{in} . Such a behavior is reversed when d is as large as 2.0 nm. This is due to the lower mass of thinner nanotubes, as gravimetric adsorption is reported (the corresponding snapshots for $d = 0.0$ and 1.0 nm are shown in Figure 8). As a net effect, the volume per CNT mass unit may have an opposite dependence as a function of R_{in} for the cases of $d \leq 0.3$ and $d \geq 1.0$, which can be rationalized by a simple calculation (see Appendix C).

The complexity of the outer adsorption in comparison to the inner adsorption (Figure 3) originates from the irregular geometry of the adsorption space and the presence of different adsorption sites. To allow a comparison between these sites, we

measure the effective density ρ^{eff} for outer adsorption (shown in Figure 10), which can be related to the details of the

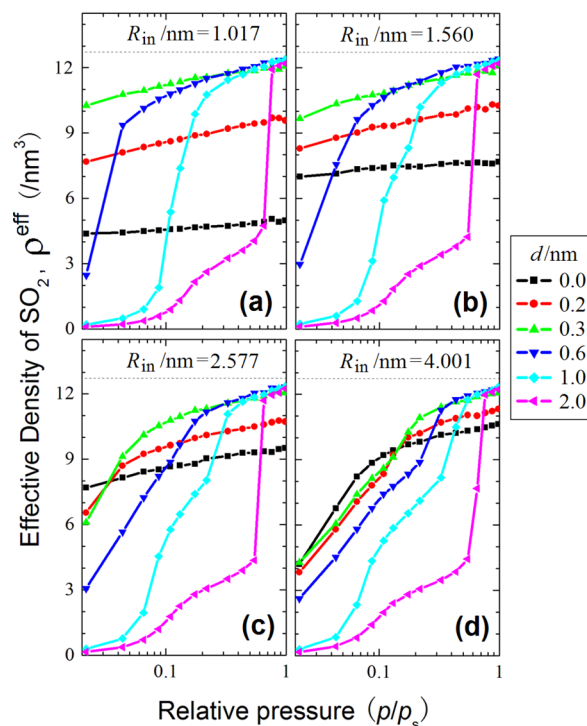


Figure 10. Effective density for the outer adsorption of SO_2 in DWCNT arrays with different nanotube radii R_{in} and intertube distances d . Dashed line represents the SO_2 bulk density at the saturation pressure (4.6 bar). Solid lines are used as a guide for the eye.

molecular packing and the extent of occupying the accessible volume. It is evident from Figure 3 that for all different R_{in} ρ^{eff} reaches a limit very close to the bulk saturation density ρ_s , subsequent to condensation/saturation. The pressure dependence of ρ^{eff} for the outer adsorption is also studied as a function of R_{in} and d . Here, the mutual dependence between ρ^{eff} and ρ_s as observed for the inner adsorption does not hold for $d < 0.3$ nm. For example, see Figure 10a and 10b. As a result of the inaccessible volume in such a limited space, the asymptotic value of ρ^{eff} for $d < 0.3$ nm is much smaller than ρ_s . Obviously, the inaccessible volume in the systems of $d = 0.0$ nm is larger than that in the systems with $d = 0.2$ nm. On the basis of these remarks we can understand that at large pressures ($p/p_s > 0.7$) the minimum ρ^{eff} is found for $d = 0.0$ nm in Figure 10a–d. The maximum ρ^{eff} for $p/p_s > 0.7$ is found in most cases when d is equal to 0.6 nm. Such an intertube distance corresponding to 2λ is just large enough to accommodate two adsorption layers between two CNTs. Thus, we have a monolayer adsorbed at each CNT surface. This interpretation is consistent with the conclusions of Yin et al. on N_2 adsorption on SWCNT.¹³

Under low-pressure conditions, the maximum ρ^{eff} is found for $d = 0.3$ nm when having $R_{\text{in}} \leq 1.560$ nm. This can be explained by the smaller inaccessible volume encountered for $d < \lambda$. Even at the lowest pressure considered in this work, the adsorption space is always completely filled when having $R_{\text{in}} \leq 1.560$ nm and $d \leq 0.3$ nm, since the adsorption energy is large and the empty room for adsorption is limited. For $R_{\text{in}} \leq 2.577$ nm, however, the maximum ρ^{eff} is realized first under $d = 0.0$ nm and then under $d = 0.3$ nm. For nanotube radii $R_{\text{in}} \leq 2.577$ nm, the empty space for adsorption at low pressures is larger

for $d = 0.3$ nm than that for $d = 0.0$ nm. When the pressure is increased and the whole adsorption space is filled, the maximum ρ^{eff} is no longer confined to $d = 0.0$ nm but occurs for $d = 0.3$ nm. This can be verified by the snapshots shown in Figure 8.

Figure 11 presents the isosteric heat of adsorption for the outer adsorption with different R_{in} and d . In Figure 6 we

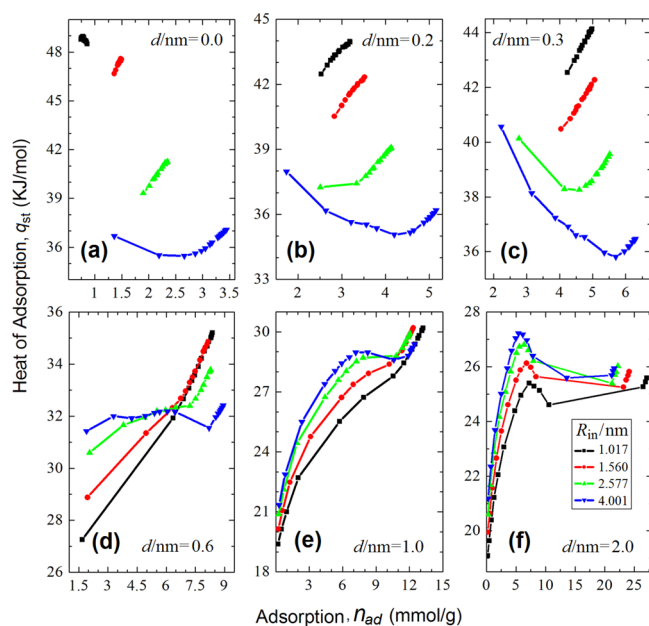


Figure 11. Isosteric heat of adsorption for the outer adsorption of SO_2 in DWCNT arrays with different nanotube radii R_{in} and different intertube distances d . Solid lines are used as a guide for the eye.

observed isotherms where the isosteric heat of adsorption q_{st} for the inner adsorption processes first increases, then decreases, and finally increases again. A similar q_{st} behavior can be observed for the outer adsorption at larger intertube distances. For a typical example see the case of $d = 2.0$ nm given in Figure 11f. For small intertube distances and nanotube radii (see Figure 11b and 11c for $d = 0.2, 0.3$ nm and $R_{\text{in}} = 1.017, 1.560$ nm), q_{st} increases monotonically with the adsorption amount (pressure). On the other hand, for the combination of a smaller d and a larger R_{in} (see Figure 11a–c for $d = 0.0, 0.2, 0.3$ nm and $R_{\text{in}} = 4.001$ nm), we observe an initial decrease and ensuing increase of q_{st} . In the case of a monotonically increasing q_{st} , we see that the adsorption space is reduced by small R_{in} and d values. In such a limited adsorption space, which can be classified as a narrow pore region, condensation occurs at very low pressures and almost the whole adsorption process occurs in stage III. This has been displayed in Figure 3 for the inner adsorption. As a result, an increase of q_{st} with the adsorption amount is observed. In other samples, such as $R_{\text{in}} = 4.001$ nm and $d = 0.3$ nm (see Figure 8), the adsorption space is large enough to allow different adsorption sites including grooves, interstitial regions, and the outer surface of CNTs. However, adsorption starts in the groove sites because of their highest adsorption energy.^{17,18,27,31} This occurs at very low pressures within a narrow pressure range. Then the adsorption continues on the outer surface of the CNTs and in the interstitial region. Finally, the adsorption space is filled at a certain pressure, and increasing pressure only leads to the insertion of SO_2 molecules and a slight increase of SO_2 density.

4.3. Data Fitting by Analytical Models. For the adsorption of SO_2 at pressures smaller than 3 bar,³² the Langmuir³⁶ and Freundlich³⁷ models can be used to accurately fit the isotherms of type I. However, these approaches are no longer valid under high-pressure conditions. Here we have fitted the adsorption isotherm data using the modified NT-PFG (eqs 4–6) and the patchwise NT-GDW (eqs 4 and 7–9) models. For all adsorption isotherms, the fit using the NT-GDW model containing 7 optimized parameters reproduces the simulation data better than the modified NT-PFG model containing 4 optimized parameters. However, the modified NT-PFG model has its own advantages. On one hand, it fits the data with sufficient accuracy as long as R_{in} and d are not too small. On the other hand, it uses fewer parameters (compared to the patchwise NT-GDW model).

A typical example is shown in Figure 12; others can be found in Supplementary Figures S2–S5. For reference, the obtained

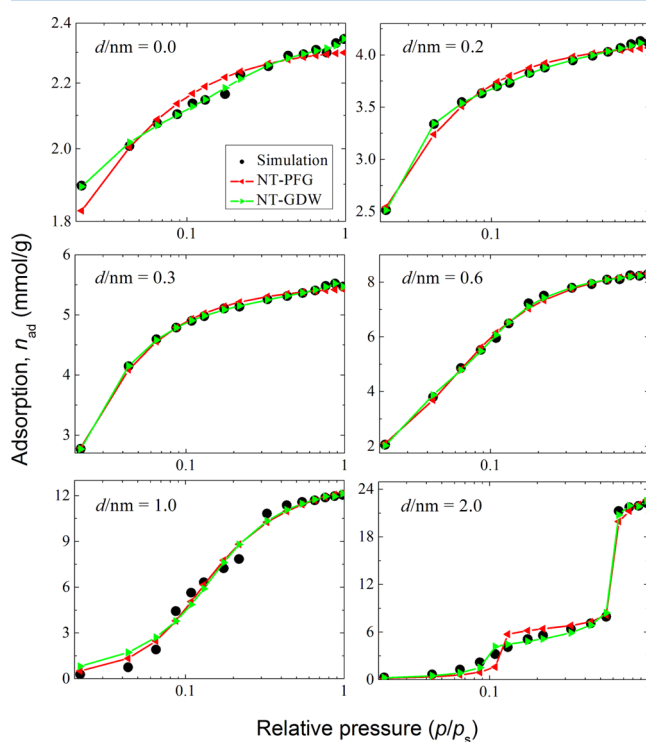


Figure 12. Results observed by fitting the data with analytical models. The plot refers to the outer adsorption in DWCNT arrays of $R_{\text{in}} = 2.577$ nm and different intertube distances d . Simulation data are shown as black dots. Red and blue triangles are based on fitting procedures within the modified NT-PFG model and the patchwise NT-GDW model. Curves are given as a guide for the eye.

parameters are presented in Tables S2–S5. From Tables S4 and S5 it can be deduced that in most cases either c or w (the multipliers in eq 7) has a very small value, which means that eq 7 does not contribute significantly to the total adsorption. Thus, here the patchwise NT-GDW model can be simplified to a bimodal model accounting for the heterogeneity of the adsorbent surface, which is similar to the one discussed by Arora et al.⁴⁰ or Terzyk et al.⁵⁴

5. CONCLUSIONS

The adsorption and condensation of SO_2 in three-dimensionally aligned hexagonal double-walled carbon nanotube arrays

have been studied at 303 K with pressures up to 98% of the saturation pressure of SO₂ in the bulk phase by grand-canonical Monte Carlo simulations. Adsorption isotherms have been determined as a function of nanotube radii $R_{in} = 1-4$ nm and intertube distances $d = 0-2$ nm. For both the inner and the outer adsorption, type I (monolayer adsorption, Langmuir Isotherm) and type IV (multilayer adsorption, condensation covered) adsorption isotherms are observed for systems with small and large adsorption spaces, respectively. These isotherms can be described accurately by simple analytical models, i.e., the patchwise NT-GDW model and the modified NT-PFG model.

The nanotube radius R_{in} and intertube distance d play an important role for the adsorption amount. Consequently, the optimal geometry of the CNT arrays for maximum adsorption strongly depends on the applied pressure. For the inner adsorption, all isotherms observed can be divided into three stages. Under low-pressure conditions in stage I, where only one monolayer is formed, the adsorption energy dominates the adsorption and the maximum adsorption is achieved for the smallest R_{in} . In stage II at intermediate pressures, where the number of adsorption layers is large, the surface area or the available volume per CNT mass unit dominates the adsorption, and thus, the maximum adsorption is achieved for the largest R_{in} . The conclusions deduced for stage II are also true for the high-pressure conditions of stage III, where the condensation transition has occurred already and the density of adsorbate is much higher than in the former two stages. However, due to the different degrees of confinement, the systems with different R_{in} do not undergo the condensation transition at the same pressure. This results in a nonlinear relation between the adsorption sequence and the nanotube radius at pressures in the vicinity of the boundary between stages II and III.

For the outer adsorption, however, the effects of R_{in} and d are much more complicated and subtle. At almost all considered pressures the adsorption is characterized by nonlinear variations as a function of R_{in} and d . The observed behavior seems to reflect this superposition of R_{in} and d . This phenomenon can also be explained on the basis of the adsorption energy and adsorption space volume per CNT mass unit. Additionally, by comparing the effective number density of SO₂ and the isosteric heat of adsorption for different systems, it has been shown that the groove regions, where one or two adsorption layers can be accommodated between two CNTs, are the most favorable adsorption sites. We hope that our simulation results and the employed analytical models can help experimentalists to design and synthesize adsorbent materials with an optimal adsorption capacity.

■ APPENDIX A: CALCULATION OF THE FREE VOLUME IN CNT ARRAYS

Different concepts and methods have been employed to calculate the free volume V^{free} from the geometry of the CNT arrays.^{13,56} In this work V^{free} is calculated from the nanotube radii (R_{in} and R_{out}) and the inaccessible radii (Δ_{in} and Δ_{out}) for carbon atoms on CNT walls. The definitions for R_{in} and R_{out} are given in Figure 1. The values of Δ_{in} and Δ_{out} are determined by a simple calculation, which is similar to but not identical to the method of Mahdizadeh and Tayyari.⁵⁶ In our model systems, SO₂ molecules cannot get closer to the CNT inner wall than 0.250 nm. Thus, we define $\Delta_{in} = \frac{0.250 \cdot \sigma_{C-C}}{\sigma_{C-C} + \sigma_{O-O}} = 0.132$ nm since the distance between a carbon and an oxygen falls into the excluded volume of both atoms. In the same way, we

have $\Delta_{out} = \frac{0.242 \cdot \sigma_{C-C}}{\sigma_{C-C} + \sigma_{O-O}} = 0.127$ nm. As a result of the curvature effect, it is found that the closest distance between a SO₂ molecule and the CNT wall for the inner case, i.e., 0.250 nm, is larger than that for outer case, i.e., 0.242 nm. This is qualitatively consistent with the results of Mahdizadeh and Tayyari.⁵⁶

With the nanotube radius and the inaccessible radius, the effective radius can be obtained as $R_{in}^{eff} = R_{in} - \Delta_{in}$ and $R_{out}^{eff} = R_{out} - \Delta_{out}$. Furthermore, the free volume for the inner regions of the CNTs in a simulation cell shown in Figure 1 can be calculated as

$$V_{in}^{free} = 2\pi(R_{in}^{eff})^2 \times L_z \quad (A1)$$

The factor 2 in eq A1 follows from the presence of two DWCNTs in one cell. Similarly, for outer free volume we have

$$V_{out}^{free} = L_x \times L_y \times L_z - 2\pi(R_{out}^{eff})^2 \times L_z \quad (A2)$$

Note that eq A2 can be used when $L_x \geq 2R_{out}^{eff}$, which is valid in this work.

■ APPENDIX B: CALCULATION OF THE SURFACE AREA OF ADSORPTION LAYER

The CNT walls in Figure A1 are shown in black. Four inner adsorption layers have been considered in the plot. The one

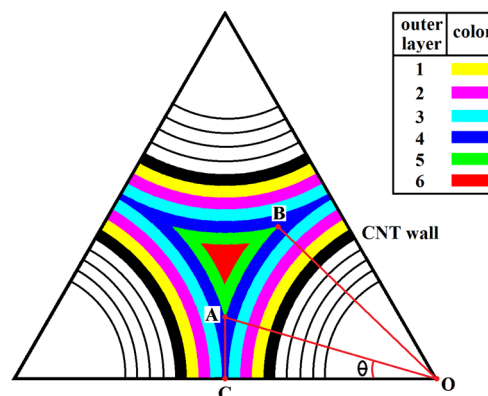


Figure A1. Schematic of multilayer adsorption on CNTs. CNT walls are in black, outer adsorptions layers are symbolized by different colors, while inner adsorptions layers are defined by empty arcs separated by black curves. The distance between O and C is denoted as L_{OC} , etc., and the angle $\angle COA$ is denoted as θ .

directly adsorbed to the CNT wall is denoted as inner layer 1, and the remaining ones are the 2–4 layers. It is obvious that for the i th inner layer the surface area of the upper surface (the interface between the i th and $(i + 1)$ th layers) is smaller than that of the bottom surface (the interface between the i th and the $(i - 1)$ th layers). This difference is described by eq 5. Similarly, eq 6 gives a correct description of the surface area for the outer adsorption layers 1, 2, and 3. However, for layer 4 the top surface of layer 3 is not available for adsorption except the part of arc AB and its analogues. The ratio of arc AB to the interface between layers 3 and 4 can be evaluated in a similar way as realized in the calculation of the free volume

$$c_\alpha = 1 - \frac{2\arccos\left[\min\left(1, \frac{L_{OC}}{L_{OA}}\right)\right]}{\pi/3} \quad (B1)$$

where $\min(\dots)$ determines the minimum value in its argument list. Equation B1 can be applied to any of the following layers.

■ APPENDIX C: CALCULATION OF THE VOLUME PER CNT MASS UNIT FOR THE OUTER ADSORPTION

Here we use a highly simplified model since only the scaling relation is important, and the picture can be imaged based on Figure A1. Assume that r is the nanotube radius and d is the van der Waals separation between the CNT walls; then the volume per CNT mass unit for the outer adsorption, V_{mass} , can be evaluated as

$$V_{\text{mass}} \approx \frac{\frac{\sqrt{3}}{4}(2r+d)^2 - \frac{\pi r^2}{2}}{\pi r} \quad (\text{C1})$$

Rewriting eq C1 we have

$$V_{\text{mass}} \approx \left(\frac{\sqrt{3}}{\pi} - 0.5 \right) r + \frac{\sqrt{3}d^2}{4\pi r} + \frac{\sqrt{3}d}{\pi} \quad (\text{C2})$$

Assume that d is constant. If the intertube distance is very small, i.e., $d/r \approx 0$, we have $V_{\text{mass}} \sim r$ by omitting the constants, which means V_{mass} increases monotonically with r . If $d/r \gg 1$, we have $V_{\text{mass}} \sim \frac{1}{r}$ and V_{mass} decreases monotonically with r . As far as intermediate r is concerned, V_{mass} does not change monotonically with r .

■ ASSOCIATED CONTENT

● Supporting Information

The Supporting Information is available free of charge on the ACS Publications website at DOI: 10.1021/acs.jpcc.5b08910.

Structural details of the model systems, fitted parameters from the analytical models, simulation data for verifying the independence on certain parameters, and fitting results with analytical models (PDF)

■ AUTHOR INFORMATION

Corresponding Author

*E-mail: yongbiao@utexas.edu.

Present Address

[§]Y.-B.Y.: Department of Chemical Engineering, University of Texas at Austin, Austin, Texas 78712, United States.

Notes

The authors declare no competing financial interest.

■ ACKNOWLEDGMENTS

We thank Sylwester Furmaniak for providing us the program codes of data fitting for their analytical models. J.K.S. also thanks the Alexander von Humboldt Foundation and Ministry of Earth Sciences, India, for financial support. This work was supported by the Priority Programme 1570 of Deutsche Forschungsgemeinschaft *Porous media with well-defined pore structure in chemical engineering: Modeling, application, synthesis*.

■ REFERENCES

- (1) Iijima, S. Helical Microtubules of Graphitic Carbon. *Nature* **1991**, *354*, 56–58.
- (2) Iijima, S.; Ichihashi, T. Single-Shell Carbon Nanotubes of 1-nm Diameter. *Nature* **1993**, *363*, 603–605.
- (3) Vela, S.; Huarte-Larrañaga, F. A Molecular Dynamics Simulation of Methane Adsorption in Single Walled Carbon Nanotube Bundles. *Carbon* **2011**, *49*, 4544–4553.

- (4) Ibrahim, K. S. Carbon Nanotubes-Properties and Applications: A Review. *Carbon Lett.* **2013**, *14*, 131–144.

- (5) Peigney, A.; Laurent, Ch.; Flahaut, E.; Bacsá, R. R.; Rousset, A. Specific Surface Area of Carbon Nanotubes and Bundles of Carbon Nanotubes. *Carbon* **2001**, *39*, 507–514.

- (6) Lafi, L.; Cossement, D.; Chahine, R. Raman Spectroscopy and Nitrogen Vapour Adsorption for the Study of Structural Changes during Purification of Single-Wall Carbon Nanotubes. *Carbon* **2005**, *43*, 1347–1357.

- (7) Kondratyuk, P.; Yates, J. T., Jr. Molecular Views of Physical Adsorption inside and outside of Single-Wall Carbon Nanotubes. *Acc. Chem. Res.* **2007**, *40*, 995–1004.

- (8) Ren, X.; Chen, C.; Nagatsu, M.; Wang, X. Carbon Nanotubes as Adsorbents in Environmental Pollution Management: A Review. *Chem. Eng. J.* **2011**, *170*, 395–410.

- (9) Cinke, M.; Li, J.; Bauschlicher, C. W., Jr.; Ricca, A.; Meyyappan, M. CO₂ Adsorption in Single-Walled Carbon Nanotubes. *Chem. Phys. Lett.* **2003**, *376*, 761–766.

- (10) Pan, B.; Xing, B. Adsorption Mechanisms of Organic Chemicals on Carbon Nanotubes. *Environ. Sci. Technol.* **2008**, *42*, 9005–9013.

- (11) Dillon, A. C.; Jones, K. M.; Bekkedahl, T. A.; Kiang, C. H.; Bethune, D. S.; Heben, M. J. Storage of Hydrogen in Single-Walled Carbon Nanotubes. *Nature* **1997**, *386*, 377–379.

- (12) Lee, S. M.; Park, K. S.; Choi, Y. C.; Park, Y. S.; Bok, J. M.; Bae, D. J.; Nahm, K. S.; Choi, Y. G.; Yu, S. C.; Kim, N.; et al. Hydrogen Adsorption and Storage in Carbon Nanotubes. *Synth. Met.* **2000**, *113*, 209–216.

- (13) Yin, Y. F.; Mays, T.; McEnaney, B. Adsorption of Nitrogen in Carbon Nanotube Arrays. *Langmuir* **1999**, *15*, 8714–8718.

- (14) Agnihotri, S.; Mota, J. P. B.; Rostam-Abadi, M.; Rood, M. J. Adsorption Site Analysis of Impurity Embedded Single-Walled Carbon Nanotube Bundles. *Carbon* **2006**, *44*, 2376–2383.

- (15) Furmaniak, S.; Terzyk, A. P.; Gauden, P. A.; Rychlicki, G. Simple Models of Adsorption in Nanotubes. *J. Colloid Interface Sci.* **2006**, *295*, 310–317.

- (16) Furmaniak, S.; Terzyk, A. P.; Gauden, P. A.; Harris, P. J. F.; Wiśniewski, M.; Kowalczyk, P. Simple Model of Adsorption on External Surface of Carbon Nanotubes - A New Analytical Approach Basing on Molecular Simulation Data. *Adsorption* **2010**, *16*, 197–213.

- (17) Kowalczyk, P.; Furmaniak, S.; Gauden, P. A.; Terzyk, A. P. Optimal Single-Walled Carbon Nanotube Vessels for Short-Term Reversible Storage of Carbon Dioxide at Ambient Temperatures. *J. Phys. Chem. C* **2010**, *114*, 21465–21473.

- (18) Rahimi, M.; Singh, J. K.; Babu, D. J.; Schneider, J. J.; Müller-Plathe, F. Understanding Carbon Dioxide Adsorption in Carbon Nanotube Arrays: Molecular Simulation and Adsorption Measurements. *J. Phys. Chem. C* **2013**, *117*, 13492–13501.

- (19) Wang, W.; Peng, X.; Cao, D. Capture of Trace Sulfur Gases from Binary Mixtures by Single-Walled Carbon Nanotube Arrays: A Molecular Simulation Study. *Environ. Sci. Technol.* **2011**, *45*, 4832–4838.

- (20) Cao, D.; Zhang, X.; Chen, J.; Wang, W.; Yun, J. Optimization of Single-Walled Carbon Nanotube Arrays for Methane Storage at Room Temperature. *J. Phys. Chem. B* **2003**, *107*, 13286–13292.

- (21) Kondratyuk, P.; Wang, Y.; Johnson, J. K.; Yates, J. T., Jr. Observation of a One-Dimensional Adsorption Site on Carbon Nanotubes: Adsorption of Alkanes of Different Molecular Lengths. *J. Phys. Chem. B* **2005**, *109*, 20999–21005.

- (22) Furmaniak, S.; Terzyk, A. P.; Rychlicki, G.; Wiśniewski, M.; Gauden, P. A.; Kowalczyk, P.; Werengowska, K. M.; Dulská, K. The System of Carbon Tetrachloride and Closed Carbon Nanotubes Analyzed by a Combination of Molecular Simulations, Analytical Modeling, and Adsorption Calorimetry. *J. Colloid Interface Sci.* **2010**, *349*, 321–330.

- (23) Rawat, D. S.; Heroux, L.; Krungleviciute, V.; Migone, A. D. Adsorption of Xenon on Purified HiPco Single Walled Carbon Nanotubes. *Langmuir* **2006**, *22*, 234–238.

- (24) Simonyan, V. V.; Johnson, J. K.; Kuznetsova, A.; Yates, J. T., Jr. Molecular Simulation of Xenon Adsorption on Single-Walled Carbon Nanotubes. *J. Chem. Phys.* **2001**, *114*, 4180–4185.
- (25) Majidi, R. Molecular Dynamics Simulation of Noble Gases Adsorption on Carbon Nanotube Bundles. *Fullerenes, Nanotubes, Carbon Nanostruct.* **2014**, *22*, S20–S27.
- (26) Zhao, J.; Buldum, A.; Han, J.; Lu, J. P. Gas Molecule Adsorption in Carbon Nanotubes and Nanotube Bundles. *Nanotechnology* **2002**, *13*, 195–200.
- (27) Bienfait, M.; Zeppenfeld, P.; Dupont-Pavlovsky, N.; Muris, M.; Johnson, M. R.; Wilson, T.; DePies, M.; Vilches, O. E. Thermodynamics and Structure of Hydrogen, Methane, Argon, Oxygen, and Carbon Dioxide Adsorbed on Single-Wall Carbon Nanotube Bundles. *Phys. Rev. B: Condens. Matter Phys.* **2004**, *70*, 035410.
- (28) Wongkoblap, A.; Do, D. D.; Wang, K. Adsorption of Polar and Non-Polar Fluids in Carbon Nanotube Bundles: Computer Simulation and Experimental Studies. *J. Colloid Interface Sci.* **2009**, *331*, 65–76.
- (29) Babu, D. J.; Lange, M.; Cherkashinin, G.; Issanin, A.; Staudt, R.; Schneider, J. J. Gas Adsorption Studies of CO₂ and N₂ in Spatially Aligned Double-Walled Carbon Nanotube Arrays. *Carbon* **2013**, *61*, 616–623.
- (30) Furmaniak, S.; Terzyk, A. P.; Golembiewski, R.; Gauden, P. A. Surface Area of Closed Carbon Nanotubes Determined from Room Temperature Measurements of Alcohols Adsorption. *Chem. Phys. Lett.* **2010**, *499*, 141–145.
- (31) Cruz, F. J. A. L.; Esteves, I. A. A. C.; Mota, J. P. B.; Agnihotri, S.; Müller, E. A. A Molecular Simulation Study of Propane and Propylene Adsorption onto Single-Walled Carbon Nanotube Bundles. *J. Nanosci. Nanotechnol.* **2010**, *10*, 2537–2546.
- (32) Rahimi, M.; Babu, D. J.; Singh, J. K.; Yang, Y.-B.; Schneider, J. J.; Müller-Plathe, F. Double-Walled Carbon Nanotube Array for CO₂ and SO₂ Adsorption. *J. Chem. Phys.* **2015**, *143*, 124701.
- (33) Cannon, J. J.; Vlucht, T. J. H.; Dubbeldam, D.; Maruyama, S.; Shiomi, J. Simulation Study on the Adsorption Properties of Linear Alkanes on Closed Nanotube Bundles. *J. Phys. Chem. B* **2012**, *116*, 9812–9819.
- (34) Liu, L.; Bhatia, S. K. Molecular Simulation of CO₂ Adsorption in the Presence of Water in Single-Walled Carbon Nanotubes. *J. Phys. Chem. C* **2013**, *117*, 13479–13491.
- (35) Liu, L.; Nicholson, D.; Bhatia, S. K. Impact of H₂O on CO₂ Separation from Natural Gas: Comparison of Carbon Nanotubes and Disordered Carbon. *J. Phys. Chem. C* **2015**, *119*, 407–419.
- (36) Langmuir, I. The Constitution and Fundamental Properties of Solids and Liquids. Part I. Solids. *J. Am. Chem. Soc.* **1916**, *38*, 2221–2295.
- (37) Freundlich, H. M. F. Über die Adsorption in Lösungen. *Z. Phys. Chem.* **1906**, *57*, 385–470.
- (38) Brunauer, S.; Emmett, P. H.; Teller, E. Adsorption of Gases in Multimolecular Layers. *J. Am. Chem. Soc.* **1938**, *60*, 309–319.
- (39) Foo, K. Y.; Hameed, B. H. Insights into the Modeling of Adsorption Isotherm Systems. *Chem. Eng. J.* **2010**, *156*, 2–10.
- (40) Arora, G.; Wagner, N. J.; Sandler, S. I. Adsorption and Diffusion of Molecular Nitrogen in Single Wall Carbon Nanotubes. *Langmuir* **2004**, *20*, 6268–6277.
- (41) Salmas, C. E.; Androutsopoulos, G. P. Rigid Sphere Molecular Model Enables an Assessment of the Pore Curvature Effect upon Realistic Evaluations of Surface Areas of Mesoporous and Microporous Materials. *Langmuir* **2005**, *21*, 11146–11160.
- (42) Aqel, A.; El-Nour, K. M. M. A.; Ammar, R. A. A.; Al-Warthan, A. Carbon Nanotubes, Science and Technology Part (I) Structure, Synthesis and Characterisation. *Arabian J. Chem.* **2012**, *5*, 1–23.
- (43) Yeow, J. T. W.; She, J. P. M. Carbon Nanotube-Enhanced Capillary Condensation for a Capacitive Humidity Sensor. *Nanotechnology* **2006**, *17*, S441–S448.
- (44) Cornell, W. D.; Cieplak, P.; Bayly, C. I.; Gould, I. R.; Merz, K. M., Jr.; Ferguson, D. M.; Spellmeyer, D. C.; Fox, T.; Caldwell, J. W.; Kollman, P. A. A Second Generation Force Field for the Simulation of Proteins, Nucleic Acids, and Organic Molecules. *J. Am. Chem. Soc.* **1995**, *117*, S179–S197.
- (45) Hummer, G.; Rasaiah, J. C.; Noworyta, J. P. Water Conduction through the Hydrophobic Channel of a Carbon Nanotube. *Nature* **2001**, *414*, 188–190.
- (46) Ketko, M. H.; Kamath, G.; Potoff, J. J. Development of an Optimized Intermolecular Potential for Sulfur Dioxide. *J. Phys. Chem. B* **2011**, *115*, 4949–4954.
- (47) Allen, M. P.; Tildesley, D. J. *Computer Simulation of Liquids*; Oxford University Press: Oxford, 1987.
- (48) Essmann, U.; Perera, L.; Berkowitz, M. L.; Darden, T.; Lee, H.; Pedersen, L. G. A Smooth Particle Mesh Ewald Method. *J. Chem. Phys.* **1995**, *103*, 8577–8593.
- (49) Ihmels, E. C.; Lemmon, E. W.; Gmehling, J. An Equation of State and Compressed Liquid and Supercritical Densities for Sulfur Dioxide. *Fluid Phase Equilib.* **2003**, *207*, 111–130.
- (50) Afeefy, H. Y.; Liebman, J. F.; Stein, S. E. Neutral Thermochemical Data. In *NIST Chemistry WebBook*; Linstrom, P. J., Mallard, W. G., Eds; NIST Standard Reference Database Number 69; National Institute of Standards and Technology: Gaithersburg, MD, <http://webbook.nist.gov> (retrieved Sept 13, 2011).
- (51) Peng, D.-Y.; Robinson, D. B. A New Two-Constant Equation of State. *Ind. Eng. Chem. Fundam.* **1976**, *15*, 59–64.
- (52) Babarao, R.; Hu, Z.; Jiang, J.; Chempath, S.; Sandler, S. I. Storage and Separation of CO₂ and CH₄ in Silicalite, C₁₆₈ Schwarzite, and IRMOF-1: A Comparative Study from Monte Carlo Simulation. *Langmuir* **2007**, *23*, 659–666.
- (53) Barton, S. S.; Evans, M. J. B.; Liang, S.; MacDonald, J. A. F. *Carbon* **1996**, *34*, 975–982.
- (54) Terzyk, A. P.; Gauden, P. A.; Rychlicki, G. Energetics of Water Adsorption and Immersion on Carbons. *Colloids Surf., A* **1999**, *148*, 271–281.
- (55) Peng, X.; Cao, D.; Wang, W. Adsorption and Separation of CH₄/CO₂/N₂/H₂/CO Mixtures in Hexagonally Ordered Carbon Nanopipes CMK-5. *Chem. Eng. Sci.* **2011**, *66*, 2266–2276.
- (56) Mahdizadeh, S. J.; Tayyari, S. F. Influence of Temperature, Pressure, Nanotube's Diameter and Intertube Distance on Methane Adsorption in Homogeneous Armchair Open-ended SWCNT Triangular Arrays. *Theor. Chem. Acc.* **2011**, *128*, 231–240.
- (57) Rouquerol, J.; Rouquerol, F.; Llewellyn, P.; Maurin, G.; Sing, K. *Adsorption by Powders and Porous Solids*; Academic Press: San Diego, CA, 1999.
- (58) Frost, H.; Düren, T.; Snurr, R. Q. Effects of Surface Area, Free Volume, and Heat of Adsorption on Hydrogen Uptake in Metal-Organic Frameworks. *J. Phys. Chem. B* **2006**, *110*, 9565–9570.